Journal of
Ceramic Science
and Technology

J. Ceram. Sci. Tech., **03** [04] 169-180 (2012)
DOI: 10.4416/JCST2012-00032
available online at: http://www.ceramic-science.com

Growth of 2M-Wollastonite Polycrystals by a Partial Melting and Recrystallization Process for the Preparation of High-Aspect-Ratio Particles

L. Zhu and H.Y. Sohn*

Department of Metallurgical Engineering, University of Utah, Salt Lake City, Utah 84112
received September 7, 2012; received in revised form October 21, 2012; accepted November 2, 2012

Abstract

A polytype of wollastonite, 2M-wollastonite, that breaks into acicular particles under external forces was synthesized in a partial melting and recrystallization process using relatively pure component materials. In the first step, samples containing SiO_2 and CaO and small amounts of various additives were pressed into discs and sintered at 1270 °C. These temperatures are lower than the melting points of the major components but higher than the melting points of most of the additives so as to partially melt the samples. The samples were then cooled to below 550 °C at an average rate of 2 – 3 K/min. At the end of this stage, alpha-wollastonite was formed and the particles produced from it displayed little or no acicularity. In the second step, when the samples were further heated at 1070 °C for 5 – 8 hours and then cooled to room temperature, 2M-wollastonite (one of the beta-wollastonite polytypes) was formed. The particles obtained from this phase displayed high acicularity with some particles having aspect ratios as high as 15:1. In addition, the effects of the types and amounts of additives, processing temperature and time on the aspect ratio of the final products were determined.

Keywords: Wollastonite, partial melting, acicular, high aspect ratio, synthesis

I. Introduction

Wollastonite has a chemical formula of $CaSiO_3$ with a theoretical composition of 48 wt% CaO and 52 wt% SiO_2. Naturally occurring wollastonite may contain trace elements such as aluminum, iron, magnesium, manganese, potassium, and sodium. It is usually white with a hardness of 4.5 to 5.5 on the Mohs scale. Both iron and manganese affect its color [1–4].

Wollastonite is a polymorphic substance and two different structural forms can be found in nature: β-wollastonite which is stable at low temperatures and α-wollastonite also called pseudo-wollastonite or cyclo-wollastonite that is stable at high temperatures. The transformation temperature from β-wollastonite to α-wollastonite was reported between 1120 °C and 1150 °C [5,6,13,14]. The β-wollastonite can be further divided into six polytypes, namely, 1T, 2M, 3T, 4T, 5T, and 7T, where M and T represent monoclinic and triclinic structure, respectively. The number here indicates the number of subcells in each unit cell of that particular polytype. These polytypes have been proposed and studied by different researchers [6–10]. Henmi *et al.* [7] listed two types of subcells. One is the normal 1T wollastonite unit cell (T) and the other is a unit cell related to T by a displacement of $b/2$. Hesse [6] suggested $d_{subcell} \approx 7.7$ Å for a unit subcell. Among the six polytypes, 2M-wollastonite, which is also named para-wollastonite, has a unique structure because it has long chains of silicon tetrahedrals [SiO_4] parallel to its *b* axis, which results in its fibrous nature [10–12].

Wollastonite powder has many useful physical and chemical properties such as low thermal expansion, low water and oil adsorption, and chemical inertness [2]. These properties make it valuable in many industrial applications such as in plastics, paints, coatings, rubbers, ceramics, refractories, and adhesives [1,15,16]. Acicular wollastonite particles act to strengthen products such as plastics, paint films and green ceramic bodies much like reinforcing rods do in concrete or similar to the effect of fiber reinforcement on the creep behavior of some metal composites such as Cu-W composites with W fibers. However, natural wollastonite usually occurs only in small amounts and is often contaminated by other minerals such as diopside, calcite, garnet and others [5]. Therefore, an interest has been aroused in research to develop synthetic wollastonite, especially wollastonite powder with high aspect ratios for all of the applications mentioned above [1,15,16]. Some recent studies have reported that synthetic wollastonite-bearing composites are found to be bioactive, making them valuable for implants and bone substitutes [17–23].

Currently, there are three types of methods for synthesizing wollastonite: the wet methods[24–27], the solid state reaction methods [28–35], and the liquid phase reaction methods [36,37]. Among these methods, the wet methods are usually performed at low temperatures (less than 200 °C), accompanied by high pressure. They can be further divided into sol-gel processing, hydrothermal reaction, and colloid

* Corresponding author: H.Y.Sohn@utah.edu

emulsion technique. The solid state reaction methods are based on the reaction of silica with calcium oxide or calcium carbonate above 800 °C. In the liquid phase reaction methods, starting mixtures are melted inside suitable crucibles at a composition close to wollastonite together with other oxides such as sodium oxide or boron oxide to lower the melting temperature. The liquid is solidified, sometimes cast into thin layers, followed by various heat treatments.

The three methods listed above have advantages and disadvantages. The wet methods can produce the highest-aspect-ratio wollastonite among the three, and also provide a means for preparing wollastonite nanowires. However, they either consume large amounts of organic solvents and templates, causing environmental and health issues [26,27], or rely on inorganic salts such as $Ca(NO_3)_2{\cdot}4H_2O$ and $Na_2SiO_3{\cdot}9H_2O$ as raw materials [25]. This makes the process relatively expensive and less flexible, and does not allow the use of cheap materials as reported in the solid state reaction methods discussed below. The latter can utilize various raw materials such as silica fume, calcite, marble waste, natural siliceous carbonates, and tailing materials. But more often they fail to produce acicular particles. None of the researchers [28–35] who used these methods reported aspect ratios of their products. We repeated experiments under similar conditions to these methods. XRD analysis proved the formation of wollastonite in the products, but the powder did not show acicular shapes. When the aspect ratio is not of significant interest, the solid state reaction methods are most efficient. The liquid phase reaction methods can produce high-aspect-ratio wollastonite powder, but the working temperature (usually greater than 1400 °C) is high. The liquid phase in this case is a mixture of acidic SiO_2 and basic CaO of 1:1 molar ratio, with some metal oxides added for various purposes. Since most refractory containers are also made of metal oxides, they tend to form complex compounds with the reactant mixture, resulting in both contamination and corrosion problems. Therefore a platinum crucible is necessary to hold these types of mixtures at temperatures above 1400 °C. The experiments by Ohsato *et al.* [36] and Kume *et al.* [37] were all carried out in platinum crucibles. In addition to the cost of platinum, the restrictions on using platinum wares at high temperatures, such as avoiding alkali oxides, iron oxides, and other unknown species, will make this method prohibitive for wollastonite production on industrial scale.

In this study, a method henceforth called the partial melting and recrystallization process was developed by combining the advantages of the solid state reaction and the liquid phase reaction methods. The purpose of creating a partially melted state is to maintain the original shape of the compacts of raw materials while melted regions form at certain points within the compacts, providing a favorable environment for the growth of wollastonite while obviating the need for a container that must withstand high-temperature contact with a corrosive melt. Currently, synthetic wollastonite accounts for less than two percent of world production of wollastonite and is mostly not of acicular type [3].

Among the processing conditions, additives (usually metal oxides) play important roles influencing the aspect ratio of synthetic wollastonite. Some oxides were reported as additives for preparing acicular wollastonite [37], but the effects of those oxides were not well established. Therefore, up to twelve additives were tested in this study.

Results show that under appropriate conditions, fine acicular particles with mean aspect ratios greater than five, including particles with aspect ratios greater than 15, were obtained. These particles were 2M-wollastonite, which is of the same crystal structure as that of high-aspect-ratio natural wollastonite particles.

II. Experimental Procedure

(1) Preparation of raw materials

Since wollastonite has a 1:1 molar ratio of SiO_2 to CaO, this ratio was adopted for the preparation of starting mixtures. The major raw materials were commercially available SiO_2 (99 %) and CaO (99 %). Various additives were tested in this study, namely, B_2O_3 (97.5 %), Al_2O_3 (99.9 %), Na_2O (88 % Na_2O, 12 % Na_2O_2), Li_2O (99.5 %), ZnO (99.1 %), Fe_2O_3 (99.9 %), MgO (96 %), MnO (99 %), BaO (88 – 94 %), Co_3O_4 (99.7 %), TiO_2 (99.9 %), and Na_2CO_3 (99.5 %). Table 1 shows the compositions of the samples used in this study. The compositions of all other samples used to determine the effects of additives and processing conditions on wollastonite synthesis are presented in the subsections where they are discussed in detail. All the chemicals mentioned above but not listed in Table 1 were purchased from Alfa Aesar, Ward Hill, MA.

Table 1: Compositions of samples

	Main components (wt%)		Additives (wt%)					
Sample	[1]SiO_2	[2]CaO	[3]B_2O_3	[3]Na_2O	[3]Al_2O_3	[4]Na_2CO_3	[3]Li_2O	[2]ZnO
1	46.8	43.2	2.7	1.8	1.8	2.7	1.0	0.0
2	46.8	43.2	2.5	2.0	2.0	2.5	1.0	0.0
3, 4	46.8	43.2	3.0	2.0	1.0	0.0	1.5	2.5

[1]Fisher Scientific, Fair Lawn, NJ; [2]J.T. Baker, Phillipsburg, NJ; [3]Alfa Aesar, Ward Hill, MA; [4]Mallinchrodt Chemicals, Phillipsburg, NJ.

The aforementioned mixtures were prepared in a laboratory mortar and pestle, and then hydraulically dry-pressed into discs at a uniaxial pressure of 300 MPa. Each disc had a diameter of 13 mm and a height of about 5 mm. To prevent the sample disc from reacting with the alumina crucible during heat treatment in the furnace, it was put on a sintered SiC disc and then placed in the crucible. The SiC discs were prepared as follows: SiC powder (600 grit) mixed with a small amount of ethylene glycol (99 %) was pressed into discs under a hydraulic pressure of 300 MPa. The green SiC discs were sintered at 1250 °C for 3 hours.

(2) Heat treatment

The raw materials were heat treated by following a typical schedule shown in Fig. 1, except in some experiments the schedule was stopped at a certain point. In the schedule, T_S stands for the temperature at which the raw material was partially melted. Its value was determined based on the deformation of the sample during the initial heat-up stage. In order to achieve this, a simple device was fabricated. The working principle is shown schematically in Fig. 2. A green filter, a monocular telescope, and a web camera with high resolution (8 MP) were placed in the order as illustrated. The web camera was connected to a computer to record the deformation of samples at different temperatures.

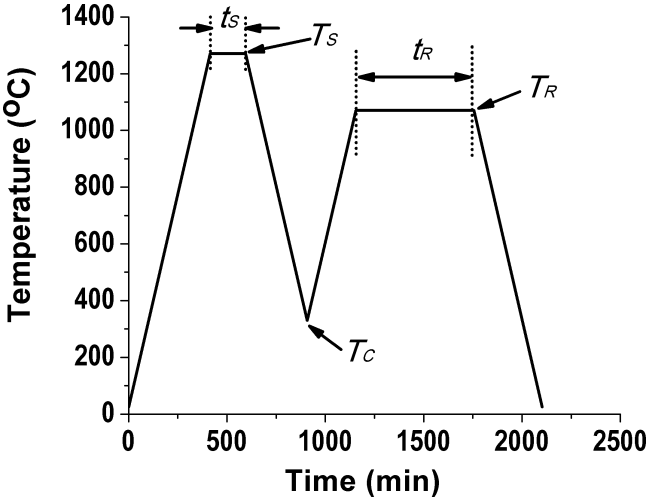

Fig. 1: Typical heating schedule.

Using the system shown in Fig. 2, the T_s of each type of mixture was determined as the temperature when its contour began to deform at an observable level, which is further divided into three stages. The first stage was when the sample had its corners gradually changing from right angles to a curved shape. In the second stage its contour tilted or bent to one side, and finally in the last stage the whole sample spread out or collapsed. The values of T_s were chosen as the temperature at which the samples were in the second stage. Fig. 3 illustrates two mixtures with different B_2O_3 contents and how they responded to the temperature increase. It is noted that the optimum T_s mainly depended on the melting point and amount of the additive. Additives like ZnO (m.p. 1975 °C) and Na_2O (m.p. 1132 °C) shifted the optimum T_s to some degree at an addition of less than 2 wt%; but the variation was usually within 15 °C when B_2O_3 (m.p. 450 °C) was present at a fixed content. Thus when determining the effects of other experimental conditions on acicularity, T_s was fixed at an average of the optimum T_s values for different additives to make the comparison simpler. Further, the holding time for sintering (t_S) was set at 3 hours based on the results of preliminary tests that showed negligible effects beyond this length of time.

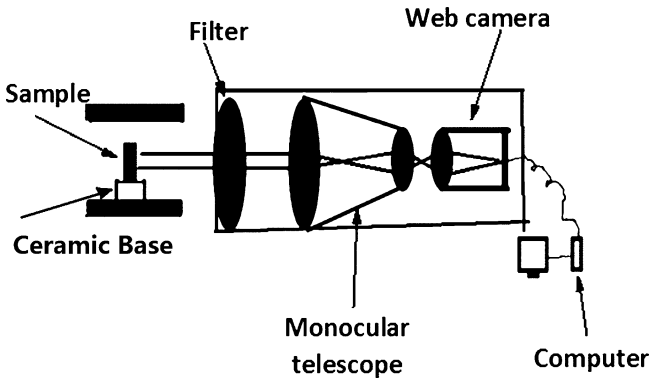

Fig. 2: Working principle of the device used to measure optimum T_S.

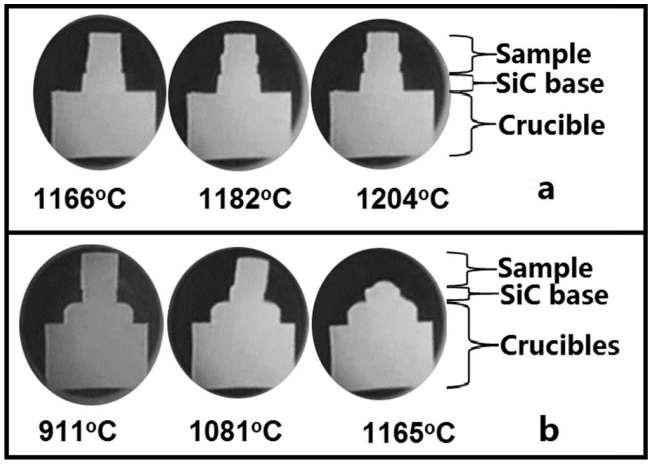

Fig. 3: Determination of optimum T_S for two samples with different compositions based on their responses to temperature increase: (a) $T_S \approx 1180$ °C; (b) $T_S \approx 1081$ °C.

After sintering, the samples were cooled to certain critical cooling temperatures designated as T_C, at which point the temperature was increased again to the recrystallization temperature (T_R) which was lower than 1120 °C (the approximate transformation temperature from alpha to beta wollastonite). The heating and cooling rates were set at no more than 3 K/min depending on the temperature ranges. In the range of 1 – 3 K/min heating and cooling rates that the furnace typically provided, these rates had negligible effects on the final products.

With T_S and t_S as well as heating and cooling rates fixed as indicated above, the aspect ratio of the synthesized wollastonite depended on the remaining three parameters, i.e. T_R, t_R, and T_C. To determine the effects of these parameters on the aspect ratios of the produced wollastonite particles, raw materials with the same composition, i.e. 47 % SiO_2, 43 % CaO, 2.5 % B_2O_3, 2 % Al_2O_3, 4 % Na_2O, and 1.5 % Li_2O by weight, were prepared and pressed into discs, as described earlier. To determine the effect of T_R, *Ts* and *Tc* were fixed at 1270 °C and 25 °C, respectively; and t_S and t_R were fixed at 3 and 8 hours, respectively. To test

the effect of t_R, *Ts*, *Tc*, and T_R were fixed at 1270 °C, 25 °C, and 1070 °C, respectively, and *ts* was fixed at 3 hours. To test the effect of *Tc*, *Ts* and $T_R$were fixed at 1270 °C and 1070 °C, respectively, and t_S and t_R were fixed at 3 and 8 hours, respectively. Table 2 lists the parameters for the heat treatments of Samples 1 to 4.

Table 2: Heat treatment schedules

Sample	Temperature (°C)			Time (hour)	
	T_S	T_R	T_C	t_S	t_R
1	1270	1000	500	3	6
2	1270	1070	300	3	8
3	1270	none	25	3	0
4	1270	1070	330	3	10

(3) Measurement of aspect ratio

After heat treatment, parts of the samples were crushed inside a cylindrical stainless steel mold by hydraulic pressure to a loose aggregate of <1 mm size particles. These particles were then placed on a well polished steel plate to form a thin layer of 0.5 to 1 mm thickness. A heavy cylindrical steel bar with a smooth surface was placed on top of the thin layer. A uniform force was then applied to the steel bar to roll it back and forth on the layer ten times. The powder was collected and screened with a series of sieves. Particles that remained on 100-mesh sieve were further ground to below 100 meshes.

The aspect ratios of the particles falling in each size range were calculated by measuring the length and width of each particle using the digital images obtained from optical microscope or SEM. In reality, particles have three dimensional needle- or rod-like shapes with the two short dimensions having similar sizes, and therefore measurement from the 2D projection images gives an average value of the short dimension. The mean aspect ratio of a given wollastonite powder was measured from five random view fields. Fig. 4 shows the procedure for measuring the mean aspect ratio from an image of an individual view field taken by SEM.

The errors in the measurement were mainly caused by crushing as well as sieving procedures [4]. Other possible factors causing errors were overlapping of particles, irregular particle shapes, and uneven sampling.

(4) Effects of additives

In order to quantitatively study the effects of additives on the aspect ratio of synthetic wollastonite particles, twelve different candidates were tested. Since some additives have higher melting points, such as MgO, and TiO_2, a higher temperature is needed to produce a partially melted phase compared with additives with lower melting points such as Na_2O. Therefore, an auxiliary additive has to be added to help generate a partially melted phase. After a few tests, B_2O_3 was determined to be the best auxiliary additive that meets the requirement, without itself promoting the formation of acicular wollastonite particles. The sintering temperature for the measurements of the effects of additives was fixed as 1270 °C. At this temperature the desired partial melting was produced for most samples with only 4 wt% B_2O_3. For some samples containing relatively high-melting-point oxides, the content of B_2O_3 had to be increased to 6 wt%. The first group contained 4 wt% B_2O_3, an additive selected from Li_2O, Al_2O_3,Na_2CO_3,Na_2O, MnO, Fe_2O_3, or-Co_3O_4, and 1:1 molar ratio of SiO_2 and CaO. The second group contained 6 wt% B_2O_3, an additive selected from ZnO, BaO, MgO, or TiO_2, and 1:1 molar ratio of SiO_2 and CaO. Each additive was added from zero percent to a level beyond which the aspect ratio remained unchanged or decreased in some cases. *Tc* and T_R were fixed at 25 °C and 1070 °C, respectively, and $t_S$and $t_R$were fixed at 3 and 5 hours, respectively, which yield good results as discussed later.

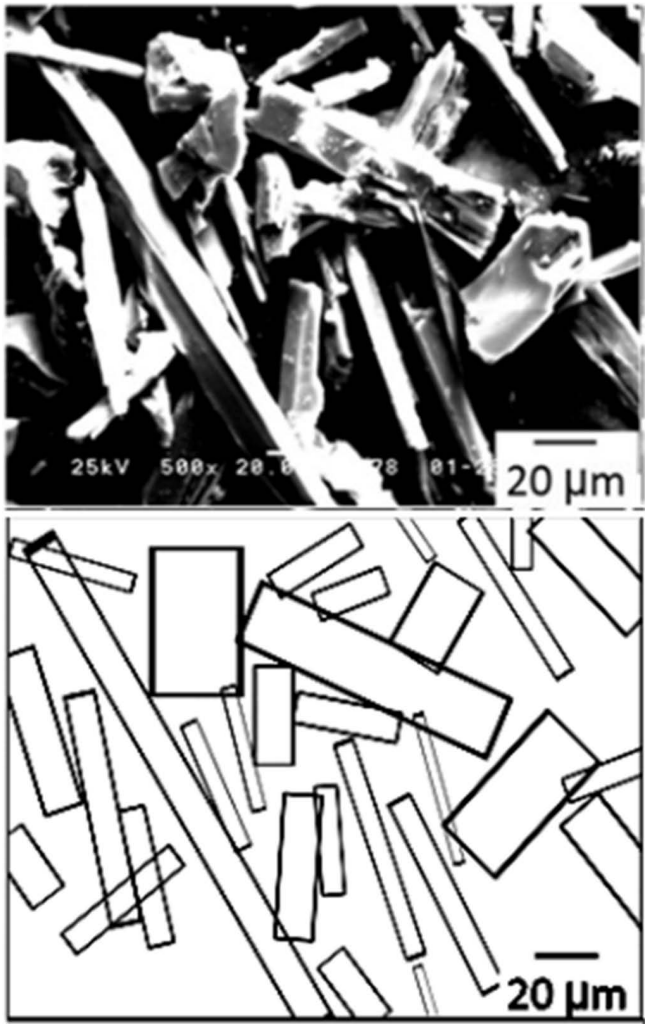

Fig. 4: Procedure used for evaluating the mean aspect ratio of wollastonite particles. The mean aspect ratio of the particles in this figure is 6.

(5) X-ray diffraction

The crystal structure of synthesized products was determined by means of X-ray diffraction (XRD) using a Siemens D5000 X-ray diffractometer, with Cu-Kα radiation, 0.02° step size, and 0.4 s scan time interval. The working voltage and current were 40 KV and 20 mA. The 2-theta scan range was from 20° to 100°. The collected

patterns were compared with those in the data files of the Joint Committee on Powder Diffraction Standards (JCPDS).

(6) SEM and optical microscope

The morphology of individual particles and the microstructure and elemental distribution of polished wollastonite samples were investigated using scanning electron microscopy (SEM, TOPCON SM-300), and optical microscope (PME3 Inverted Metallurgical Microscope, Olympus). For polished samples, they were prepared by regular metallographic techniques and etched with 10 vol% HF solution for 15 ~ 20 seconds.

III. Results and Discussion

(1) XRD, SEM, and optical microscope analysis

Fig. 5 shows that the major crystalline phase in natural wollastonite (NW) particles that present high aspect ratios is 2M-wollastonite. The major phase in wollastonite product with sintering only (SW) is alpha-wollastonite. The major phase in the product with both sintering and recrystallization treatment (SRW) is 2M-wollastonite, which is the same as in natural wollastonite. Comparing the standard XRD pattern of 2M wollastonite (JCPDS 43 – 1460) with that of natural wollastonite, one can see a relative intensity change for some peaks corresponding to planes of (400) and (600), which belong to 100 plane series. It is known that beta wollastonite has good cleavage along 100 planes [4, 36]. Therefore, under external forces, more faces from 100 planes of 2M wollastonite will be exposed, resulting in strong peaks occurring at 100 planes, which agrees with the XRD observation. While the SRW product also shows the preferred cleavage along 100 plane series, it has additional preferred cleavage along ($\bar{2}02$) planes. If we add a proper additive that prevents the cleavage of the SRW product along ($\bar{2}02$) planes and at the same time promotes the cleavage along 100 plane series, we might be able to produce better products.

Corresponding to the difference in crystal structures, we found that the fracture surfaces of the SW and the SRW products also have different properties. The exposed fracture surfaces of the SW samples were relatively smooth, while the SRW samples had a rough fracture surface, as shown in Fig. 6.

Under the exposure to light source with changing direction, the fracture surfaces of the SW products showed nearly even reflection of light from different areas. The fracture surfaces of the SRW products, however, showed some areas that are brighter than the surrounding areas, as shown in Fig. 6. These brighter areas mostly had rectangular shapes with a maximum length of about 4 mm, and a maximum width of about 2 mm. By varying the incident light direction, new brighter spots were reflected, while the previous ones disappeared. Some preliminary explanation for this phenomenon is given as follows: 2M wollastonite has good cleavage along certain planes just like mica. When exposed to incident light, these planes display directional reflection of the incident light because of their perfect smoothness. Compared with 2M wollastonite, alpha wollastonite does not have planes with good cleavage. As a consequence, a beam of incident light will be reflected much more weakly from such a fracture surface, making the reflection diffusive.

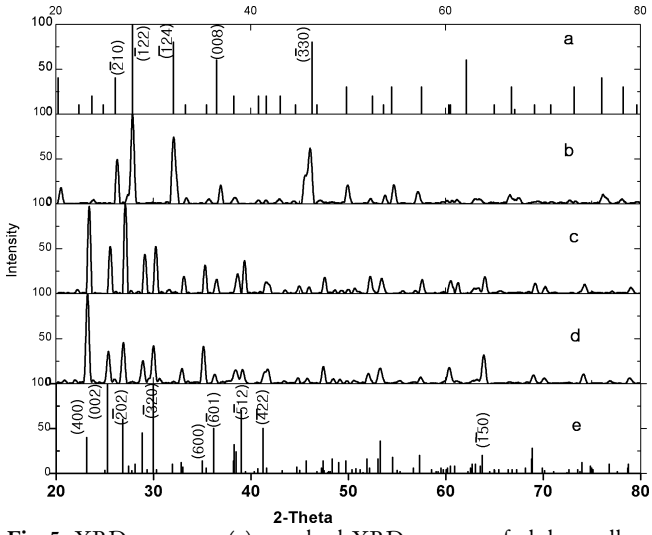

Fig. 5: XRD patterns: (a) standard XRD pattern of alpha-wollastonite (also called cyclowollastonite, JCPDS 10 – 486); (b) product with sintering only (SW) - Sample 3; (c) product with both sintering and recrystallization treatments (SRW) - Sample 4; (d) natural wollastonite (NW) from NYCO Company (NYGLOS®12); (e) standard XRD pattern of 2M-wollastonite (JCPDS 43 – 1460).

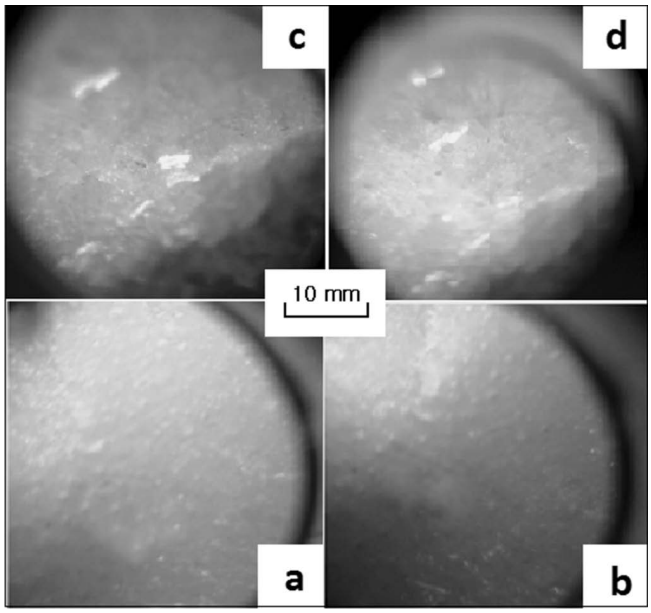

Fig. 6: Reflection of incident light from fracture surfaces of: (*a* and *b*) a product with sintering treatment only (SW) - Sample 3; [The entire surface displays diffuse reflection.]; (*c* and *d)* a product with both sintering and recrystallization treatments (SRW) - Sample 4. [Lighter areas show directional reflection from the cleavage planes.]

Knowing this difference can actually help estimate the aspect ratios of particles obtained from an uncrushed product with relatively good accuracy. If no shining crystals or planes are seen under light exposure, it is almost certain that no acicular particles will be created after crushing the bulk sample. On the contrary, if the whole fracture surface is distributed by those shining crystals, it is likely that acicular particles will be obtained, and the bigger the crystals or planes are, the higher the mean aspect ratios will be. By

using this method, it is possible to make a quick and preliminary evaluation with regard to the final products without crushing and sieving, making it useful for the synthesis of wollastonite on industrial scale if the partial melting and recrystallization process is adopted.

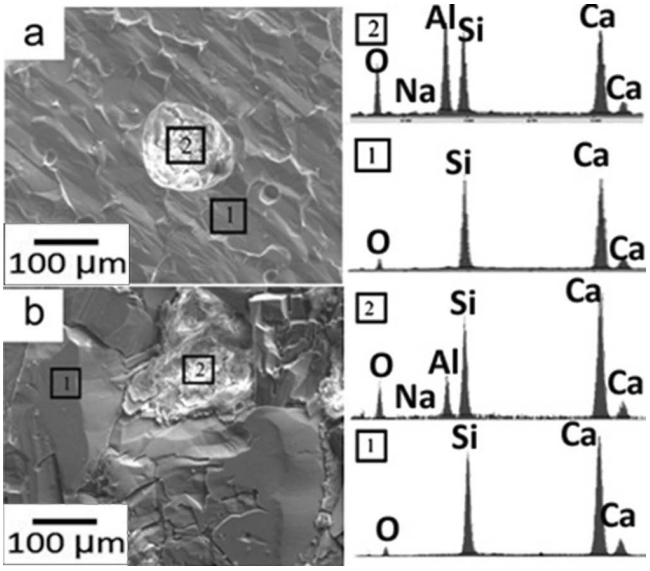

Fig. 7: SEM images and EDX analysis of samples: (a) with sintering treatment only (SW) -Sample 3 and (b) with both sintering and recrystallization treatments (SRW) -Sample 4. Both samples were etched for 15 ~ 20 seconds with 10 vol% HF solution.

As shown in Fig. 7, both the SW and the SRW products have a second phase dispersed in the main matrix. Energy Dispersive X-ray Spectroscopy (EDX) results indicate that the major phases in both products have a nearly 1:1 molar ratio of Si to Ca, which conforms to the chemical formula of wollastonite, i.e. $CaSiO_3$. The low content of oxygen is due to its light atomic weight. It is also noted that aluminum, and sodium concentrate in grain corners and pores. However, lithium and boron are not seen either in the major phase or in the defects, which is probably due to their light atomic weights.

(2) Particle morphology

The particle shapes of raw materials and the crushed synthetic wollastonite (SRW) particles are compared in Fig. 8. As clearly shown in Figs. 8a to 8g, all raw materials show either spherical or polygonal shapes with aspect ratios nearly 1:1 except Al_2O_3 particles (Fig. 8b) presenting some trigonal shapes. The crushed wollastonite particles (from Sample 4), however, show mainly acicular shapes with varying aspect ratios (Fig. 8h). The optical microscope image shows that these acicular particles are semi-transparent with the two longest edges along the major axis parallel to each other, as shown in Fig. 9. Particle 1 in Fig. 9 shows an aspect ratio of about 30:1, which is nearly the highest aspect ratio we had ever observed. Compared with Particle 1 and 2, Particle 3 shows not only smaller aspect ratios but also irregular shapes, making it look like a soft agglomeration. Initially we thought this particle might be a cluster of small particles. However, these clusters of particles with irregular shapes were also observed with SEM in similar products. With EDX analysis, we found that these particles with irregular shapes were not wollastonite particles most of the time.

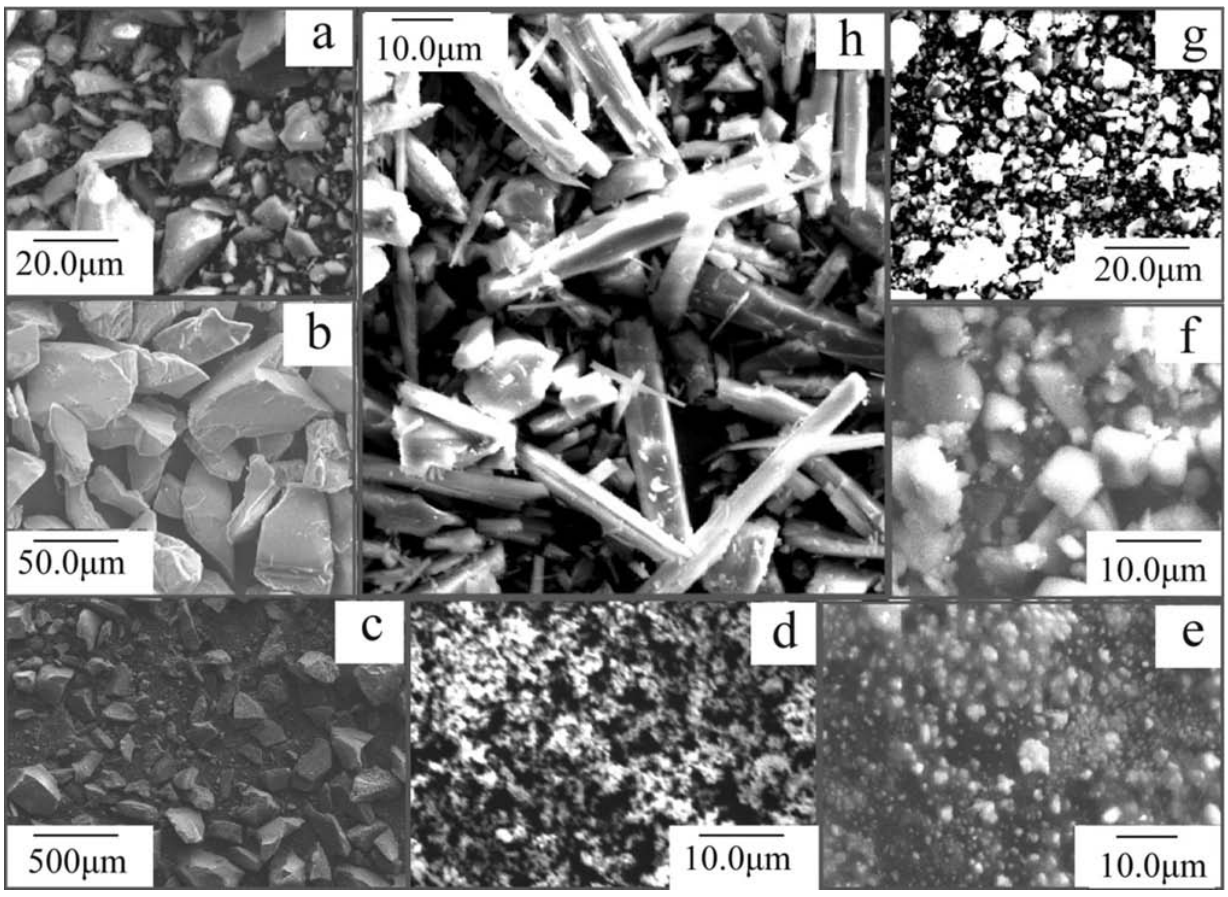

Fig. 8: shapes of: (a) SiO_2, (b)Al_2O_3, (c) B_2O_3, (d) ZnO, (e)Na_2O (12% Na_2O_2), (f) Li_2O, (g) CaO, (h) Synthetic wollastonite (Sample 4).

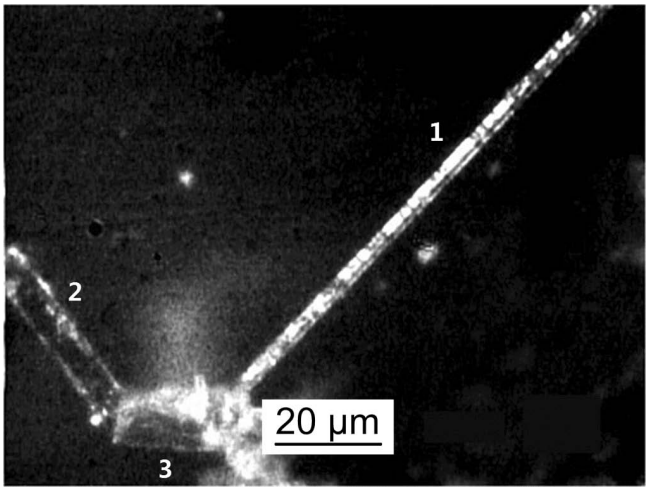

Fig. 9: Three particles collected from Sample 1 coincidently made up a check mark. Particles 1, 2, and 3 have aspect ratios of 30:1, 5:1, and 2:1, respectively. These particles are semi-transparent under an optical microscope.

Four view fields corresponding to four different particles from Sample 2 were analyzed by means of SEM and EDX as shown in Fig. 10. Two of the four particles have regular shapes, while the other two have irregular shapes. The particles with regular shapes show nearly equal contents of calcium and silicon, and no other metal elements were observed. The particles with irregular shapes show not only calcium and silicon, but also sodium and aluminum at small percentages, which agrees with their small addition during raw materials preparation. The carbon peaks were introduced by the carbon tape used to attach the sample particles. Though these irregular shape particles usually make up less than 5 % in number percentages, because of their nearly 1:1 aspect ratios, their effects on reducing the mean aspect ratios of the synthetic wollastonite and how to remove them effectively will be investigated in our future study.

As seen from Figs. 11a through 11d, particles obtained from products with sintering only (SW) have a nearly 1:1 aspect ratio in the range of 38 to 150 μm. Some particles smaller than 38 μm have a 2:1 to 3:1 aspect ratios, as shown in Figs. 11e, and 11f, but the average aspect ratio is still very low.

The aspect ratios of particles obtained from products with both sintering and recrystallization treatments (SRW) are between 2:1 to 5:1 for the size range of 75 to 150 μm, as shown in Figs. 12a, and 12b. While the aspect ratio of the particles in the range of 38 to 75 μm is about 3:1 to 8:1, it increases to 5:1 to 15:1 for the particles smaller than 38 μm.

The difference in the aspect ratio between the SW and the SRW particles can be explained by their microstructures as shown in Fig. 13. The SW particles have a smooth fracture surface with no obvious cracks or faults on the surface. These particles look like tiny hard stones, as seen in Figs. 13a, and 13b. The SRW particles have straight parallel cracks and stacking faults extending along the major axis, as seen in Figs. 13c, and 13d. When particles with such cracks or faults are pressed under external forces, they are much easier to break into more acicular particles, making them different from the SW particles.

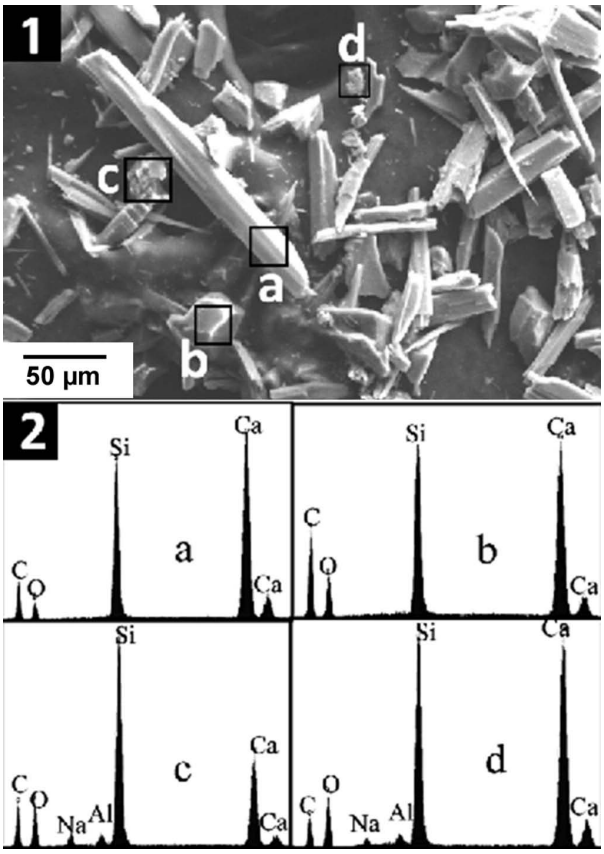

Fig. 10: SEM images presenting particles obtained from a recrystallized product (Sample 2): (1*a* and 1*b*) particles with regular shapes; (1*c* and 1*d*) particles with irregular shapes; (2*a* to 2*d*) EDX spectrum of particles 1*a* to 1*d*. While only calcium and silicon are observed as metal elements in the particles with regular shapes, additional metal elements including sodium and aluminum appear in the particles with irregular shapes.

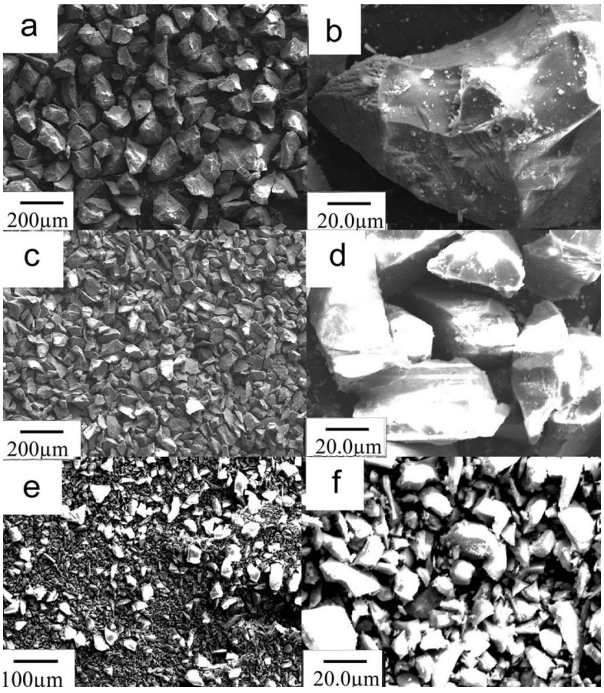

Fig. 11: SEM images of particles obtained from product with sintering only (SW) -Sample 3: (*a* and *b*) size range of 75 ~ 150 μm under low and high magnification; (*c* and *d*) size range of 38 ~ 75 μm under low and high magnification; (*e* and *f*) size range below 38 μm under low and high magnification.

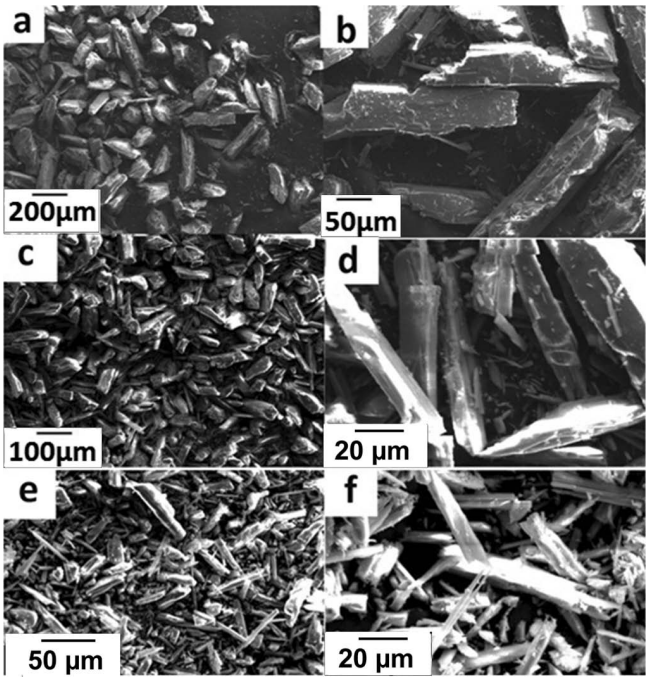

Fig. 12: SEM images of particles obtained from product with both sintering and recrystallization treatments (SRW) -Sample 4: (*a* and *b*) size range of 75 ~ 150 μm under low and high magnification (15.2 wt%); (*c* and *d*) size range of 38 ~ 75 μm under low and high magnification (40.3 wt%); (*e* and *f*) size range of below 38 μm under low and high magnification (44.5 wt%).

(3) Effects of additives on aspect ratio

As shown in Fig. 14, additives play different roles influencing the mean aspect ratio of wollastonite particles. It is clearly shown that particles obtained from products containing one of the four additives, namely B_2O_3 (melting point 450 °C), Na_2CO_3 (melting point 851 °C), Na_2O (melting point 1132 °C), and Al_2O_3 (melting point 2072 °C), have mean aspect ratios that are nearly 1:1. However, compared with the other three additives whose melting points are lower than the applied sintering temperature (usually 1270 °C), Al_2O_3 has a much higher melting point. Therefore, it is unlikely that Al_2O_3 can help form a partially melted phase. But when added with one or more of the other three additives together, Al_2O_3-containing discs shrank much more in dimensions compared with the discs containing only the other three additives, resulting in a denser sintered disc with lower porosity.

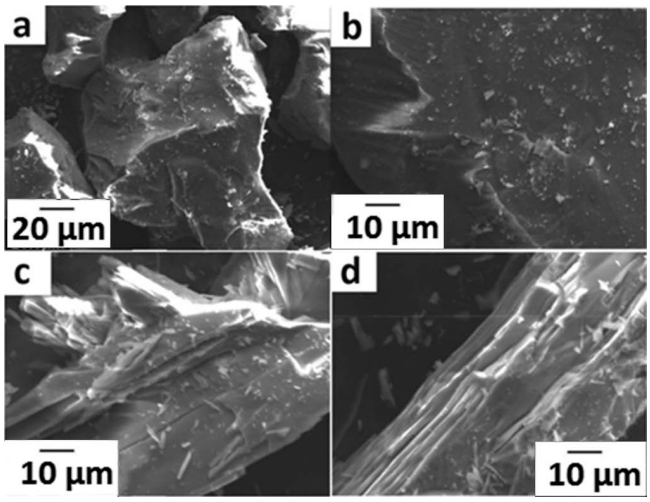

Fig. 13: SEM images of individual particles in the size range of 75 ~ 150 μm: (*a* and *b*) two random particles from product with sintering only (SW) -Sample 3, they have a smooth fracture surface with no obvious cracks on the surface; (*c* and *d*) two random particles from product with both sintering and recrystallization treatments (SRW) -Sample 4, presenting parallel cracks and stacking faults extending along the major axis.

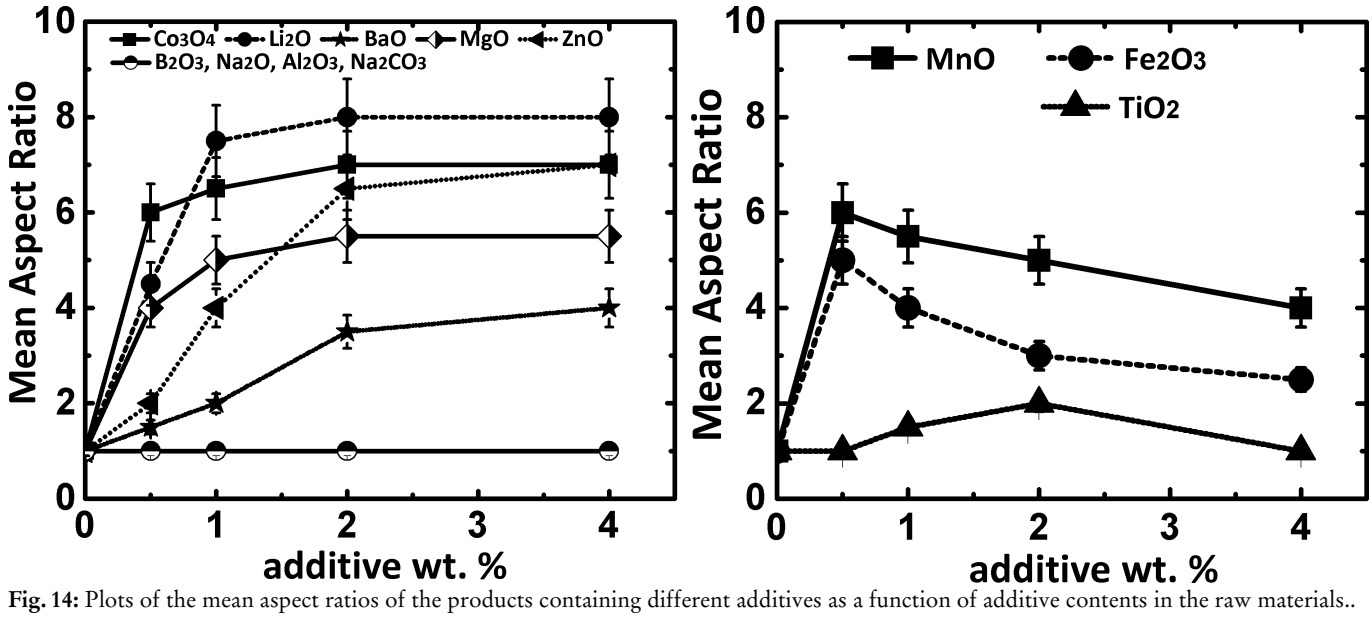

Fig. 14: Plots of the mean aspect ratios of the products containing different additives as a function of additive contents in the raw materials..

The remaining eight additives, Li_2O, Co_3O_4, MnO, Fe_2O_3, BaO, MgO, TiO_2, and ZnO, all promote the formation of acicular wollastonite particles, but they show different efficiencies with regard to their influence on the mean aspect ratios of wollastonite particles. In general, the mean aspect ratios of the particles containing one of the eight additives increase with increasing additive content, and gradually level off at about 2 wt%, except MnO-, TiO_2-, and Fe_2O_3-containing particles showing a decrease in mean aspect ratios to some degree after they reach the maximum effect, as shown in Fig. 14. Taking the experimental error into consideration, the three exceptions follow a similar trend as that of the other five additives, which means the effects of additives on the mean aspect ratio of wollastonite particles will saturate at low levels and will no longer increase the mean aspect ratio if added in excess. Among the eight additives, particles containing Li_2O, ZnO, Co_3O_4 show the highest maximum mean aspect ratios, followed by particles containing MgO, MnO, and Fe_2O_3 as having medium mean aspect ratios. Particles containing TiO_2 and BaO show the lowest mean aspect ratios among the eight. However, products containing Co_3O_4, MnO, and Fe_2O_3 have blue, pink and brown appearances, respectively, with only 0.5 wt% addition, while products containing other additives are white in appearance. Products with colorized appearances may not be acceptable for use as commercial wollastonite substitutes, such as in plastic and paint applications.

Based on the description above, these additives are classified into three groups. The first one is melting-point-depressing additives, which lower the melting point of the starting mixture significantly in a small amount (less than 10 wt%). These oxides are B_2O_3, Na_2O, and Na_2CO_3. The second group is regulatory additives, which do not lower the melting point of the mixture significantly or help produce acicular wollastonite particles, but modify the properties of the sintered products, such as reducing the pores in the products resulting in a higher density. Al_2O_3 is one of these additives. The third group is catalytic additives, which promote or accelerate the formation of acicular wollastonite. Such additives are Li_2O, ZnO, Co_3O_4, MgO, MnO, Fe_2O_3, BaO, and TiO_2. Considering the maximum mean aspect ratios and appearances, Li_2O, ZnO, MgO were determined to be the best catalytic additives among the tested additives.

(4) Effects of heat treatment on aspect ratio

Fig. 15 shows the relationship between the mean aspect ratio of each sample and the recrystallization temperature. As seen from the figure, under the same recrystallization time, the optimum recrystallization temperature is between 1050 °C to 1070 °C. When temperature is below or above this range, the mean aspect ratio of the products decreases noticeably. When temperature is close to 1120 °C, which is the approximate transformation temperature of wollastonite from the beta phase to the alpha phase, the products show nearly no acicular properties. At a lower temperature, the nucleation and growth of 2M wollastonite from alpha wollastonite is thermodynamically favorable, but from the kinetic point, it is unfavorable compared with a higher recrystallization temperature, resulting in a lower mean aspect ratio under the given recrystallization time. At a higher temperature close to the transformation temperature from beta to the alpha phase, the kinetic factor is high, but the nucleation of 2M wollastonite and its growth are thermodynamically restricted, therefore one will see reduced mean aspect ratios at the higher temperature side in the plot.

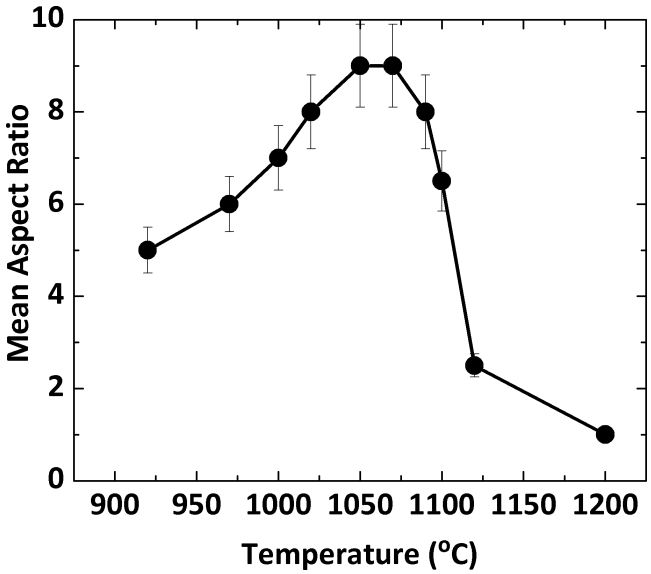

Fig. 15: The relationship between the mean aspect ratio and recrystallization temperature. T_s = 1270 °C, T_c = 25 °C, t_S = 3 h, t_R = 8 h.

As seen from Fig. 16, initially the mean aspect ratio of the tested samples increases rapidly with increasing recrystallization time, and then it reaches the maximum level after 8 hours of recrystallization treatment. A longer recrystallization time doesn't increase the mean aspect ratio significantly.

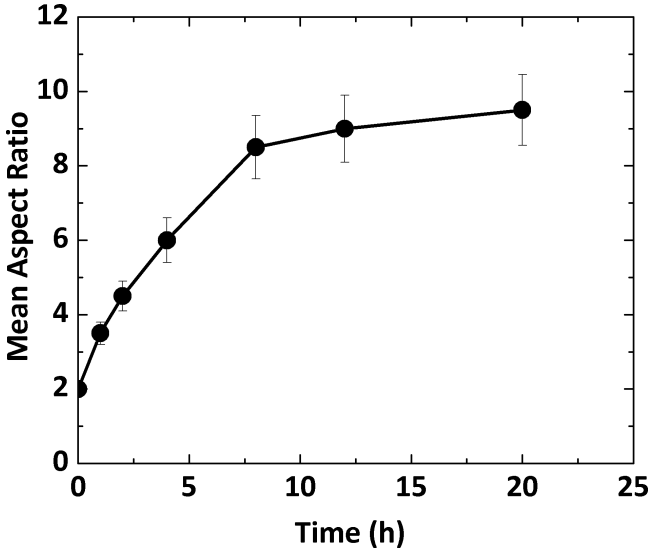

Fig. 16: The relationship between the mean aspect ratio and recrystallization time. T_s = 1270 °C, T_R = 1070 °C, T_c =25 °C, t_S = 3 h.

It was noticed when the sintered products were cooled from temperatures above 1200 °C with a cooling rate less than 3 °C/min and then went through recrystallization

stage directly, the products failed to yield acicular particles after being crushed. However, the same raw materials yielded acicular particles under the same heat treatment except that they were cooled to room temperature before entering the recrystallization stage. In order to verify this observation, we did a series of tests which were described in detail in the Experimental Procedure section.

As seen in Fig. 17, when the critical cooling temperature is above 970 °C, the mean aspect ratio of the particles obtained from the tested samples is nearly 1:1. When the critical cooling temperature is between 550 °C and 970 °C, the mean aspect ratio of the particles obtained from the tested samples is quite sensitive to temperature change. If the critical cooling temperature is decreased further to below 550 °C, the mean aspect ratio of the tested samples remains almost unchanged, meaning the critical cooling temperature has a negligible effect on the mean aspect ratio, or in other words the mean aspect ratio is insensitive to the critical cooling temperature under this condition. Therefore, a critical cooling temperature of lower than 550 °C is necessary to form acicular wollastonite particles in an efficient way under the fixed recrystallization temperature and time.

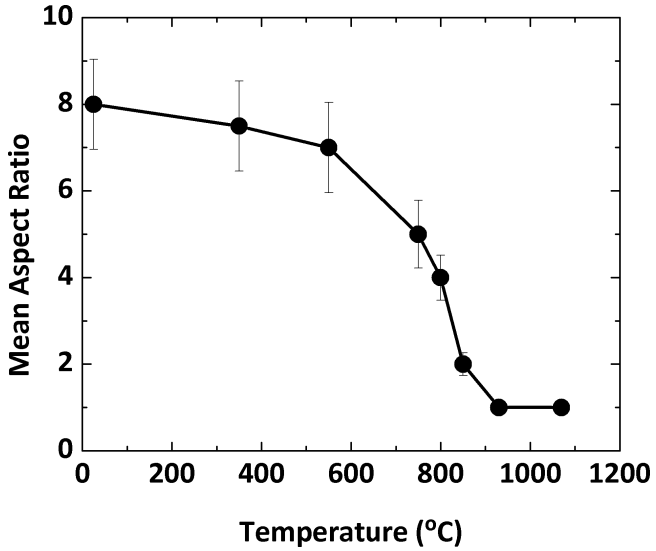

Fig. 17: The relationship between the mean aspect ratio and critical cooling temperature. T_s = 1270 °C, T_R = 1070 °C, t_S = 3 h, t_R = 8 h.

Combining the cooling temperature and recrystallization process which includes recrystallization temperature and time, one conclusion is drawn in that when the critical cooling temperature is satisfied, the recrystallization process controls the mean aspect ratio. Conversely, if the cooling temperature is not sufficient, it will dominate the final product.

The dependence of the mean aspect ratio on the critical cooling temperature indicates that it is thermodynamically unfavorable for the nucleation of 2M wollastonite from alpha wollastonite matrix when the temperature is above 970 °C. Knowing this can help to better understand the relationship between the mean aspect ratios of tested particles with recrystallization time. Nucleation of 2M wollastonite starts at a lower temperature and the newly formed nuclei begin to grow slowly while the temperature starts increasing. The growth of these crystals becomes faster when the temperature rises closer to the recrystallization temperature (for t_R test, T_R = 1070 °C). Upon reaching the recrystallization temperature (t_R = 0), the crystals are still small compared with those crystals given enough recrystallization time (t_R > 8 h). At this point, 2M wollastonite crystals occupy a small volume fraction of the whole matrix, resulting in a mean aspect ratio of slightly greater than 1 at t_R = 0. Because of this small volume fraction, the space surrounding a 2M wollastonite crystal is sufficient for further growth. Therefore, they will grow fast, resulting in a rapid increase of the volume fraction of 2M wollastonite, which explains the increase in the mean aspect ratios of the tested samples with increasing recrystallization time in the first few hours (t_R < 5 h) under the fixed recrystallization temperature. After 5 hours, the 2M wollastonite crystals have dominated the matrix, and they begin to compete with each other for space. It becomes harder for the crystals to grow larger, and this competition contributes to the slow increase in the mean aspect ratio during this period (5 < t_R < 8 h). The recrystallization from alpha wollastonite to 2M wollastonite will complete upon the depletion of alpha wollastonite, resulting in a nearly unchanged mean aspect ratio with increasing time (t_R> 8 h), as shown in Fig. 16.

IV. Conclusions

High-aspect-ratio wollastonite powder was successfully prepared by using the partial melting and recrystallization process. This process was found to be simple to synthesize wollastonite powder without completely melting the raw materials; it is especially advantageous when high acicularity of the final product is desired. The results further indicated the following:

1. The synthetic wollastonite produced without recrystallization treatment was alpha-wollastonite, whereas 2M-wollastonite was formed with both sintering and recrystallization treatments. While alpha-wollastonite yielded low-aspect-ratio wollastonite particles, 2M wollastonite yielded particles with aspect ratios as high as 15:1.

2. 2M wollastonite particles have straight parallel cracks or stacking faults extending from one end of the particle to the other end. When particles with such cracks or faults are pressed under applied stress, they are much easier to break into more acicular particles, making them different from alpha wollastonite particles.

3. Additives play important roles in the preparation of high-aspect-ratio wollastonite particles. B_2O_3 is a good additive to lower the melting point of the raw mixtures. Al_2O_3 can adjust the properties of the raw mixtures if added with other additives together. Li_2O, ZnO, and MgO are some good additives that promote the formation of acicular wollastonite particles.

4. Heat treatment is critical to the aspect ratios of synthetic wollastonite particles. A heat treatment schedule with a sintering temperature of 1270 °C; a recrystallization temperature between 1050 °C and 1070 °C; a critical cooling temperature of lower than 550 °C; with the sintering and recrystallization time no less than 3 and 8 hours, respectively, was determined to yield a product with a high aspect ratio.

Acknowledgments

The authors wish to thank Messrs. Pei Sun, Chai Ren, Tyler Bronson, and Sadegh Safarzadeh of University of Utah for their help with the SEM work, XRD analysis, and helpful technical discussion. Mr Salvatore LaRosa, Technical Marketing Manager of NYCO Minerals Inc., supplied the natural wollastonite samples used in this research and provided comments regarding synthetic wollastonite products, which is gratefully acknowledged. Mr Robert L. Virta of USGS offered help on the applications of natural wollastonite products. This work was supported in part by the U.S.-Egypt Science and Technology Joint Fund in cooperation with U.S. National Science Foundation and the Academy of Scientific Research and Development of Egypt under NSF Grant No. OISE 0913513/MAN10011354-F1. Liangzhu Zhu received a scholarship from the China Scholarship Council during the course of this work.

References

1 Virta, R.L.: Wollastonite – a versatile industrial mineral, *U.S.Geol. Surv. Fact Sheet FS- 002–01,* (2011).

2 Virta, R.L.: Wollastonite. *U.S. Geol. Surv., Annual Publications* 83.1–83.2, (1999).

3 Hawley, G.C.: Wollastonite, *Min. Eng.,* **62** [6], 84–87, (2010).

4 Ma, Z.X., Li, H., Gai, G.S., Hu, X.F.: The present situation and conception of milling technology for preparation of needle-like wollastonite powder. *Bull. Chin. Ceram. Soc.,* no. 6, 42–45, (2000).

5 Kotsis, I., Balogh, A.: Synthesis of wollastonite, *Ceram. Int.,* **15**, [2], 79–85, (1989).

6 Hesse, K.F.: Refinement of the crystal structure of wollastonite-2M (parawollastonite). *Z. Kristallogr.,* **168**, 93–8, (1984).

7 Henmi, C., Kawahara, A., Henmi, K., Kusachi, I., Takeuchi, Y.: The 3T, 4T and 5T polytypes of wollastonite from kushiro, hiroshima prefecture, japan, *Am. Mineral.,* **68**, [1–2] 156–63, (1983).

8 Henmi, C., Kusachi, I., Kawahara, A., Henmi, K.: 7T wollastonite from fuka, okayama prefecture, *Mineral. J.,* **9** 169–81, (1978).

9 Ito, T., Sadanada, R., Takeuchi, Y., Tokonami, M.: The existence of partial mirrors in wollastonite, *Proc. Jpn. Acad.,* **45** 913–8 (1969).

10 Tolliday, J.: Crystal structure of β-wollastonite. *Nature,* **182**, [4641] 1012–13 (1958).

11 Jefferson, D.A., Thomas, J.M., Smith, D.J., Camps, R.A., Catto, C.J.D., Cleaver, J.R.A.: Individual silicate chains in wollastonite by high resolution electron microscopy, *Nature,* **281**, [5726], 51–52, (1979).

12 Trojer, F.J.: The crystal structure of parawollastonite, *Z. Kristallogr.,* **127**, [1–4], 291–308, (1968).

13 Phillips, B., Muan, A.: Phase equilibria in the system CaO-iron oxide-siO2 in air, *J. Am. Ceram. Soc.,* **42**, [9], 413–23, (1959).

14 Morais. L.V., Fonseca, A.T.: Kinetics of isothermal solid state reaction of β-wollastonite synthesis from natural raw materials, *Br. Ceram. T.*, **96**, [2], (1997).

15 NYCO Mineral. Inc. NYCO literature. Available at http://nycominerals.com/our-directories/nyco-literature

16 R. T. Vanderbilt Company. Comprehensive Minerals Applications Guide. Available at http://www.rtvanderbilt.com/rubber_11_5.htm.

17 Pattanayak, D.K., Prasad, R.C., Rao, B.T., Mohan T.R.R.: Apatite wollastonite-titanium biocomposites: synthesis and in vitro evaluation, *J. Am. Ceram. Soc.,* **89**, [7] 2172–76, (2006).

18 Faeghi-Nia, A., Marghussian, V.K., Taheri-Nassaj, E., Pascual M.J., Durán A.: Pressureless sintering of apatite/wollastonite-phlogopite glass-ceramics, *J. Am. Ceram. Soc.,* **92**, [7], 1514–18, (2009).

19 Carrodeguas, R.G., De Aza, A.H., De Aza, P.N., Baudín, C., Jiménez, J., López-Bravo, A., Pena, P., De Aza, S.: Assessment of natural and synthetic wollastonite as source for bioceramics preparation, *J. Biomed. Mater. Res. Part A,* **83A,** [2], 484–95, (2007).

20 De Aza, P.N., Luklinska Z.B., Anseau, M.R., Guitian, F., De Aza, S.: Bioactivity of pseudowollastonite in human saliva, *J. Dent.,* **27**, [2], 107–13, (1999).

21 Kokubo, T., Shigematsu, M., Nagashima, Y., Tashiro, M., Nakamura, T., Yamamuro, T., Higashi, S.: Apatite- and wollastonite-containg glass-ceramics for prosthetic application, *Bull. Inst. Chem. Res.,* Kyoto Univ., **60,** [3–4], 260–68, (1982).

22 Juhasz, J.A., Best, S.M., Bonfield, W., Kawashita, M., Miyata, N., Kokubo, T., Nakamura, T.: Apatite-forming ability of glass-ceramic apatite-wollastonite-polyethylene composites: effect of filler content, *J. Mater. Sci.: Mater. M.,* **14,** [6], 489–95, (2003).

23 Cannillo, V., Pierli, F., Sampath, S., Siligardi, C.: Thermal and physical characterisation of apatite/wollastonite bioactive glass-ceramics, *J. Eur. Ceram. Soc.,* **29**, [4], 611–19, (2009).

24 Huang, X.H., Chang, J.: Synthesis of nanocrystalline wollastonite powders by citrate-nitrate gel combustion method, *Mater. Chem. Phys.,* **115**, [1], 1–4, (2009).

25 Lin, K.L., Chang, J., Chen G.F., Ruan, M.L., Ning, C.Q.: A simple method to synthesize single-crystalline β-wollastonite nanowires, *J. Cryst. Growth,* **300**, [2], 267–71, (2007).

26 Li, X.K., Chang, J.: Synthesis of wollastonite single crystal nanowires by a novel hydrothermal route, *Chem. Lett.,* **33**, [11], 1458–59, (2004).

27 Lin, K.L., Chang, J., Lu, J.X.: Synthesis of wollastonite nanowires via hydrothermal microemulsion methods, *Mater. Lett.,* **60**, 3007–10, (2006).

28 Nizami, M.S., Farooq, M.K., Hussain, K., Iqbal, M.Z.: Solid state reaction yielding a mineral utilizing silica obtained from an agricultural waste, *J. Mater. Sci. Technol.,* **15**, [03], 276–80, (1999).

29 Kartal, A., Akpinar, S.: Synthesis of wollastonite by using various raw materials. *Key Eng. Mat.,* **264–268**, 2469–72, (2004).

30 Saltevskaya, L.M., Livson, Z.A., Ryshchenko, M.I.: Synthesis of wollastonite and its use in ceramic bodies, *Glass Ceram.,* **31**, [2], 114–17, (1974).

31 Balkevich, V.L., Peres, F.S., Kogos, A.Y., Kliger, A.B., Fishman, M.A.: Synthesizing wollastonite from natural siliceous carbonate compositions, *Glass Ceram.,* **42**, [1], 40–43, (1985).

32 Emrullahoğlu, S.B., Emrullahoğlu, Ö.F., Emrullahoğlu, C.B.: Synthetic wollastonite production from raw and tailing materials, *Key Eng. Mat.,* **264 – 268,** 2485–88, (2004).

33 Yun, Y.H., Yun, S.D., Park, H.R., Lee, Y.K., Youn, Y.N.: Preparation of β-wollastonite glass-ceramics, *J. Mater. Synth. Proces.,* **10**, [4], 205–09, (2002).

34 Jacob, C.J.: Synthesis of wollastonite from natural materials without fusion, U.S. Patent No. 3,966,884, (1976).

35 Vichaphund, S., Kitiwan, M., Atong, D., Thavorniti, P.: Microwave synthesis of wollastonite powder from eggshells, *J. Eur. Ceram. Soc.,* **31**, [14], 2435–40, (2011).

36 Ohsato, H., Sugimura, T.: Morphology of synthetic β-wollastonite and para-wollastonite, *J. Cryst. Growth,* **74**, [3], 656–58, (1986).

37 Kume, M., Mizuno, T.: Glass composition suitable for production of fibrous wollastonite, method for producing said wollastonite, and wollastonite obtained thereby. U.S. Patent No. 4,443,550, (1984).